Electronic Supplementary Material (ESI) for Journal of Materials Chemistry A.

Unravelling thermal stress due to thermal expansion mismatch in metal-organic frameworks for methane storage

Jelle Wieme and Veronique Van Speybroeck*

Center for Molecular Modeling, Ghent University, Tech Lane Ghent Science Park Campus A, Technologiepark 46, 9052 Zwijnaarde, Belgium

E-mail: Veronique.VanSpeybroeck@UGent.be

S1 Materials

System-specific force fields were derived for various MOFs as listed in Tables S1, S2, S3 and S4.

Table S1: Al-based metal-organic frameworks under study.

MOF	ρ ($kg \cdot m^{-3}$)	ASA ($m^2 \cdot g^{-1}$)	Void fraction (%)	LCD (Å)	α_0 (MK^{-1})	β_0 (GPa)	γ ($MPa \cdot K^{-1}$)
Al-soc-MOF-1[1]	343	5010	79	15.9	-13.3	8.9	-0.118
MOF-519[2]	894	1163	32	8.7	-14.9	10.2	-0.152
MOF-520[2]	529	3793	69	10.1	-12.8	7.8	-0.100
MOF-520-BPDC[3]	605	3158	62	10.4	-10.3	13.0	-0.133

Table S2: Zn-based metal-organic frameworks under study.

MOF	ρ ($kg \cdot m^{-3}$)	ASA ($m^2 \cdot g^{-1}$)	Void fraction (%)	LCD (Å)	α_0 (MK^{-1})	β_0 (GPa)	γ ($MPa \cdot K^{-1}$)
IRMOF-8[4]	424	4662	81	17.7	-40.3	4.9	-0.196
IRMOF-10[4]	304	5244	86	21.5	-47.6	4.9	-0.233
MOF-5 (IRMOF-1)[5]	555	3993	77	15.5	-36.7	11.1	-0.408
MOF-177[6]	406	4895	80	11.9	-30.3	6.2	-0.187
MOF-180[7]	242	6358	87	16.5	-131.4	1.4	-0.179
MOF-200[7]	204	6335	89	17.9	-39.1	3.7	-0.145
MOF-205 (DUT-6)[7,8]	361	5211	83	23.1	-29.3	7.4	-0.218
MOF-210[7]	223	6028	88	31.6	-96.6	1.6	-0.155
MOF-905[9]	500	4024	79	19.8	-106.9	3.9	-0.415
MOF-950[9]	550	4155	76	9.8	-26.0	9.2	-0.239
MUF-7[10]	364	4863	81	22.0	-25.2	6.8	-0.171
UMCM-1[11]	366	4587	83	25.2	-40.9	5.9	-0.240
UMCM-8[12]	490	4337	79	16.2	-26.3	6.3	-0.166
UMCM-9[12]	362	5009	83	19.1	-37.5	4.7	-0.175

Table S3: Zr-based metal-organic frameworks under study.

MOF	ρ ($kg \cdot m^{-3}$)	ASA ($m^2 \cdot g^{-1}$)	Void fraction (%)	LCD (Å)	α_0 (MK^{-1})	β_0 (GPa)	γ ($MPa \cdot K^{-1}$)
NU-800[13]	567	4458	75	13.9	-80.6	4.1	-0.331
pbz-MOF-1[14]	630	3360	66	14.6	-10.6	10.8	-0.114

Table S4: Cu-based metal-organic frameworks under study.

MOF	ρ ($kg \cdot m^{-3}$)	ASA ($m^2 \cdot g^{-1}$)	Void fraction (%)	LCD (Å)	α_0 (MK^{-1})	β_0 (GPa)	γ ($MPa \cdot K^{-1}$)
FJI-H5[15]	415	4385	80	22.1	-18.9	1.7	-0.031
HKUST-1[16]	851	2229	66	13.5	-9.7	20.7	-0.199
HNUST-2[17]	555	4604	73	11.5	-32.5	4.7	-0.152
MFM-112[18]	475	4200	77	22.7	-14.4	11.6	-0.167
MOF-505 (NOTT-100)[19,20]	888	2422	64	10.2	-10.8	20.2	-0.219
NJU-Bai 10[21]	652	3404	71	12.9	-13.5	6.3	-0.085
NJU-Bai 17[22]	789	2942	67	10.2	-12.1	15.5	-0.187
NJU-Bai 19[23]	680	3293	68	11.2	-9.7	13.9	-0.135
NJU-Bai 41[24]	708	2902	65	11.9	-9.6	9.9	-0.095
NJU-Bai 42[24]	664	3483	71	11.8	-7.5	11.1	-0.083
NOTT-101[25]	657	3384	71	11.7	-10.1	14.3	-0.145
NOTT-108[25]	749	2730	66	11.6	-7.7	15.4	-0.117
NU-111[26]	390	4704	80	23.4	-58.1	5.7	-0.330
NU-125[27]	550	3795	74	19.9	-11.8	6.4	-0.075
NU-135[28]	721	2803	62	11.8	-9.2	13.3	-0.122
NU-140[29]	367	4979	81	25.0	-17.1	2.0	-0.035
PCN-11[30]	714	3112	70	10.7	-17.8	18.0	-0.320
PCN-14[31]	786	2353	56	11.7	-4.8	14.5	-0.070
PCN-61[32]	537	3795	74	20.2	-37.0	10.6	-0.392
PCN-66[32]	413	4726	80	22.9	-50.9	5.4	-0.274
PCN-68 (NOTT-116)[33,34]	355	5113	81	25.7	-42.0	6.6	-0.276
PCN-610 (NU-100)[33,35]	274	5876	86	28.9	-107.4	1.6	-0.171
UTSA-20[36]	885	2085	58	10.4	-9.7	8.0	-0.078
UTSA-61[37]	690	2834	68	17.5	-17.7	17.9	-0.318
UTSA-76[38]	669	3288	71	11.5	-7.8	13.5	-0.106
UTSA-80[39]	676	2837	64	13.7	-17.2	8.6	-0.147
UTSA-88[40]	831	2412	62	11.6	-9.9	13.8	-0.137
UTSA-110[41]	571	4021	74	12.8	-15.8	7.5	-0.119
ZJU-5[42]	664	3309	71	11.6	-11.5	14.6	-0.167
ZJU-32[43]	420	4759	80	16.2	-23.0	6.3	-0.146
ZJU-35[44]	630	3190	74	15.0	-13.5	12.8	-0.173
ZJU-36[44]	489	3948	78	17.5	-38.6	3.0	-0.146

S2 Extra figures and tables

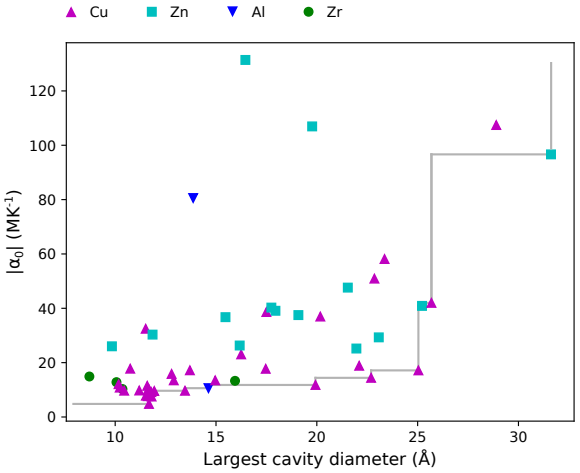

Figure S1: The magnitude of the thermal expansion coefficient as a function of the largest cavity diameter. A Pareto front where the thermal expansion coefficient is minimized and the largest cavity diameter is maximised is shown.

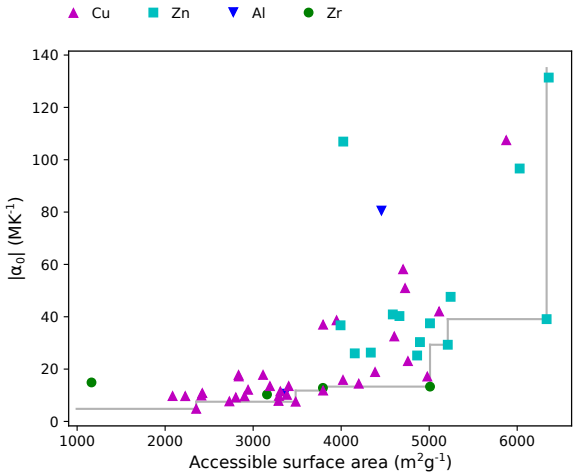

Figure S2: The magnitude of the thermal expansion coefficient as a function of the accessible surface area. A Pareto front where the thermal expansion coefficient is minimized and the accessible surface area is maximised is shown.

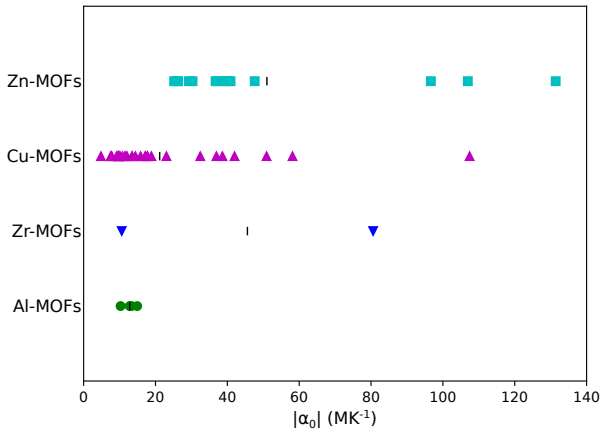

Figure S3: Influence of the inorganic building block on the thermal expansion coefficient. The vertical black line indicates the average per inorganic building block.

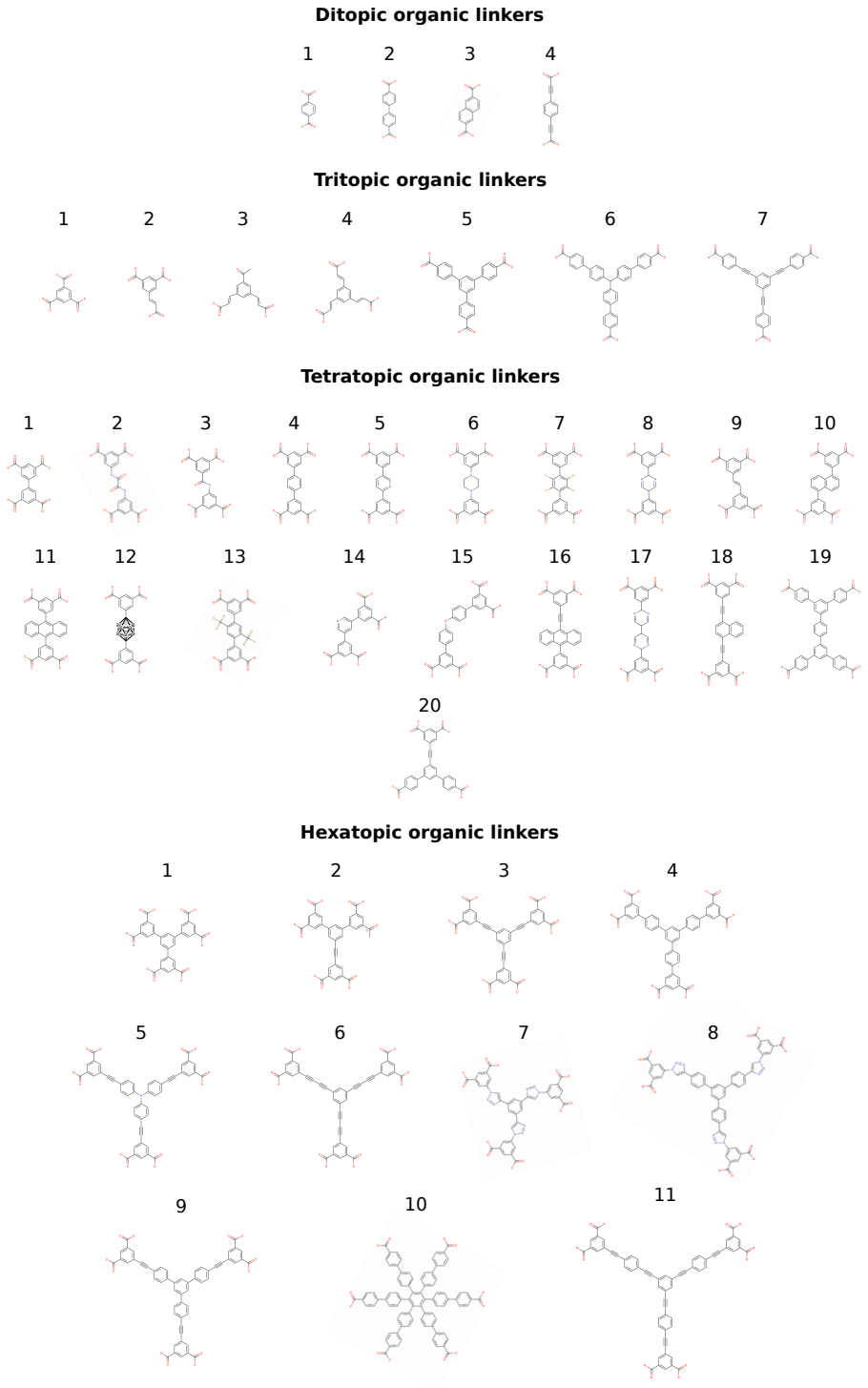

Figure S4: Overview of the organic linkers used in this work. The hydrogens are implicit.

Table S5: Organic linkers of the Al-based metal-organic frameworks under study (Figure S4).

MOF	Ditopic	Tritopic	Tetratopic	Hexatopic
Al-soc-MOF-1[1]	-	-	19	-
MOF-519[2]	-	5	-	-
MOF-520[2]	-	5	-	-
MOF-520-BPDC[3]	2	5	-	-

Table S6: Organic linkers of the Zn-based metal-organic frameworks under study (Figure S4).

MOF	Ditopic	Tritopic	Tetratopic	Hexatopic
IRMOF-8[4]	3	-	-	-
IRMOF-10[4]	2	-	-	-
MOF-5 (IRMOF-1)[5]	1	-	-	-
MOF-177[6]	-	5	-	-
MOF-180[7]	-	7	-	-
MOF-200[7]	-	6	-	-
MOF-205 (DUT-6)[7,8]	3	5	-	-
MOF-210[7]	2	7	-	-
MOF-905[9]	1	4	-	-
MOF-950[9]	-	4	-	-
MUF-7[10]	1, 2	5	-	-
UMCM-1[11]	1	5	-	-
UMCM-8[12]	1, 3	-	-	-
UMCM-9[12]	2, 3	-	-	-

Table S7: Organic linkers of the Zr-based metal-organic frameworks under study (Figure S4).

MOF	Ditopic	Tritopic	Tetratopic	Hexatopic
NU-800[13]	4	-	-	-
pbz-MOF-1[14]	-	-	-	10

Table S8: Organic linkers of the Cu-based metal-organic frameworks under study (Figure S4).

MOF	Ditopic	Tritopic	Tetratopic	Hexatopic
FJI-H5[15]	-	-	15	-
HKUST-1[16]	-	1	-	-
HNUST-2[17]	-	-	18	-
MFM-112[18]	-	-	-	4
MOF-505 (NOTT-100)[19,20]	-	-	1	-
NJU-Bai 10[21]	-	-	14	-
NJU-Bai 17[22]	-	-	3	-
NJU-Bai 19[23]	-	-	6	-
NJU-Bai 41[24]	-	-	10	-
NJU-Bai 42[24]	-	-	2	-
NOTT-101[25]	-	-	4	-
NOTT-108[25]	-	-	7	-
NU-111[26]	-	-	-	6
NU-125[27]	-	-	-	7
NU-135[28]	-	-	12	-
NU-140[29]	-	-	-	8
PCN-11[30]	-	-	9	-
PCN-14[31]	-	-	11	-
PCN-61[32]	-	-	-	3
PCN-66[32]	-	-	-	5
PCN-68 (NOTT-116)[33,34]	-	-	-	9
PCN-610 (NU-100)[33,35]	-	-	-	11
UTSA-20[36]	-	-	-	1
UTSA-61[37]	-	-	-	2
UTSA-76[38]	-	-	8	-
UTSA-80[39]	-	-	16	-
UTSA-88[40]	-	-	13	-
UTSA-110[41]	-	-	17	-
ZJU-5[42]	-	-	5	-
ZJU-32[43]	-	-	20	-
ZJU-35[44]	-	2	-	-
ZJU-36[44]	-	3	-	-

S3 Force field simulations

The first-principles force fields used to model the systems under study are derived using `QuickFF`.[45,46] Within this protocol, the quantum mechanical potential energy surface (PES) is approximated by a sum of analytical functions of the nuclear coordinates that describe the covalent (cov) and noncovalent (noncov) interactions. The latter are composed of electrostatic and van der Waals interactions. The force field and a structure are added for every MOF in Yaff-format as supplementary information.

$$V^{FF} = \underbrace{V_{bond} + V_{bend} + V_{oopd} + V_{torsion} + V_{cross}}_{V_{cov}} + \underbrace{V_{ei} + V_{vdW}}_{V_{noncov}}. \tag{S3.1}$$

S3.1 First-principles cluster data

The required first-principles cluster data for the determination of the covalent terms in the force field are generated with `Gaussian 16`[47] using the B3LYP[48] exchange-correlation functional. A 6-311G(d,p) basis set[49] is used for all row 1, row 2 and row 3 atoms, together with the LanL2DZ basis set for Zn and Zr.[50] The atomic charges are derived with the Minimal Basis Iterative Stockholder (MBIS) partitioning scheme[51] from the all-electron density obtained with `Gaussian 16`. The atomic charges of the Zn- and Zr-clusters are obtained from the PBE[52] all-electron density computed with `GPAW`[53]. The force field parameters for the atom types overlapping in the organic linker and the inorganic brick cluster models were averaged.

S3.2 Covalent interactions

The covalent interactions – which mimic the chemical bonds between the atoms – are approximated by different terms as a function of the internal coordinates (bonds, bends, out-of-plane distances, and dihedrals). The unknown force field parameters are fitted following the `QuickFF` procedure.[45] We use an extended version[46] to include anharmonic bond and bend terms,[54] which are important when modeling nuclear quantum effects and the thermal expansion of MOFs.[55,56] The anharmonic bond and bend terms are given by:

$$V_{\text{bond}}^{ij} = \frac{K_{ij}}{2}\left(r_{ij} - r_{0,ij}\right)^2 \left[1 - \alpha\left(r_{ij} - r_{0,ij}\right) + \frac{7}{12}\cdot\alpha^2\cdot\left(r_{ij} - r_{0,ij}\right)^2\right], \tag{S3.2}$$

$$V_{\text{bend}}^{ijk} = \frac{K_{ijk}}{2}\left(\theta_{ijk} - \theta_{0,ijk}\right)^2 \Big[1 - a_1\left(\theta_{ijk} - \theta_{0,ijk}\right) + a_2\cdot\left(\theta_{ijk} - \theta_{0,ijk}\right)^2 - a_3\cdot\left(\theta_{ijk} - \theta_{0,ijk}\right)^3 + a_4\left(\theta_{ijk} - \theta_{0,ijk}\right)^4\Big], \tag{S3.3}$$

with $\alpha = 2.55$ Å^{-1}, $a_1 = 0.014$ deg^{-1}, $a_2 = 5.6\cdot10^{-5}$ deg^{-2}, $a_3 = 7\cdot10^{-7}$ deg^{-3}, and $a_4 = 2.2\cdot10^{-8}$ deg^{-4}. We also add cross terms between the bonds and bends to improve the correspondence with the first-principles data.[55] The included cross terms are:

- angle stretch-stretch terms (ASS) between neigboring bonds, i.e. part of the same angle
- angle stretch-angle terms (ASA).

The mathematical expression of these terms is given by

$$V_{\text{ASS}}^{ijk} = K_{ijk}^{\text{ASS}}\left(r_{ij} - r_{0,ij}\right)\left(r_{jk} - r_{0,jk}\right) \tag{S3.4}$$

$$V_{\text{ASA}}^{ijk} = \left[K_{ijk}^{\text{ASA1}}\left(r_{ij} - r_{0,ij}\right) + K_{ijk}^{\text{ASA2}}\left(r_{jk} - r_{0,jk}\right)\right]\left(\theta_{ijk} - \theta_{0,ijk}\right). \tag{S3.5}$$

The out-of-plane distances are described using a harmonic potential:

$$V_{oopd}^{ijkl} = \frac{K_{ijkl}}{2}\left(d_{ijkl} - d_{0,ijkl}\right)^2. \tag{S3.6}$$

This is a four-atom interaction, in which the internal coordinate is the distance between the central atom and the plane determined by its three neighbors. The fourth covalent

term is the dihedral energy term. Here, a cosine term is used as a function of the dihedral angle, including the multiplicity m_ϕ of the dihedral angle:

$$V_{torsion}^{ijkl} = \frac{K_{ijkl}}{2}\left[1 - \cos(m_\phi(\phi_{ijkl} - \phi_{0,ijkl}))\right]. \tag{S3.7}$$

The unknown parameters in all terms (force constants, rest values, and multiplicities) in the covalent energy expression can be estimated directly with `QuickFF`.

S3.3 Electrostatic interactions

The electrostatic interactions are modeled by a Coulomb interaction between Gaussian charge distributions,[57] which allows to include all pairwise interactions. The atomic charges q_i are derived with the Minimal Basis Iterative Stockholder (MBIS) partitioning scheme.[51]

$$V_{ei} = \frac{1}{2}\sum_{\substack{i,j=1 \\ (i\neq j)}} \frac{q_i q_j}{4\pi\epsilon_0 r_{ij}} \operatorname{erf}\left(\frac{r_{ij}}{d_{ij}}\right) \tag{S3.8}$$

Gaussian charge distributions are used with a total charge q_i and radius d_i, centered on atom i. The mixed radius of the Gaussian charges,[57] d_{ij}, is given by $\sqrt{d_i^2 + d_j^2}$. The interaction depends on the distance r_{ij} between the two atoms.

S3.4 Van der Waals interactions

The van der Waals interactions are described by the MM3-Buckingham model[58,59] up to a finite cutoff (12 Å) and are supplemented with tail corrections.[60]

$$V_{vdW} = \epsilon_{ij}\left[1.84 \cdot 10^5 \exp\left(-12\frac{r}{\sigma_{ij}}\right) - 2.25\left(\frac{\sigma_{ij}}{r}\right)^6\right] \tag{S3.9}$$

The two parameters σ_{ij} and ϵ_{ij} are the equilibrium distance and the well depth of the potential. These parameters are typically determined with empirical mixing rules for the interaction between atom i and atom j:

$$\sigma_{ij} = \sigma_i + \sigma_j \qquad \text{and} \qquad \epsilon_{ij} = \sqrt{\epsilon_i \epsilon_j} \tag{S3.10}$$

and these parameters were taken from the MM3 force field for every atom and are tabulated in Ref. 59. In MM3, the 1-2 and 1-3 interactions are discarded to avoid a strong overestimation of the repulsion terms.

References

(1) Alezi, D.; Belmabkhout, Y.; Suyetin, M.; Bhatt, P. M.; Weselinski, L. J.; Solovyeva, V.; Adil, K.; Spanopoulos, I.; Trikalitis, P. N.; Emwas, A.-H.; Eddaoudi, M. MOF Crystal Chemistry Paving the Way to Gas Storage Needs: Aluminum-Based soc-MOF for CH_4, O_2, and CO_2 Storage. *J. Am. Chem. Soc.* **2015**, *137*, 13308–13318.

(2) Gándara, F.; Furukawa, H.; Lee, S.; Yaghi, O. M. High Methane Storage Capacity in Aluminum Metal-Organic Frameworks. *J. Am. Chem. Soc.* **2014**, *136*, 5271–5274.

(3) Kapustin, E. A.; Lee, S.; Alshammari, A. S.; Yaghi, O. M. Molecular Retrofitting Adapts a Metal-Organic Framework to Extreme Pressure. *ACS Cent. Sci.* **2017**, *3*, 662–667.

(4) Eddaoudi, M.; Kim, J.; Rosi, N.; Vodak, D.; Wachter, J.; O'Keeffe, M.; Yaghi, O. M. Systematic Design of Pore Size and Functionality in Isoreticular MOFs and Their Application in Methane Storage. *Science* **2002**, *295*, 469–472.

(5) Li, H.; Eddaoudi, M.; O'Keeffe, M.; Yaghi, O. M. Design and Synthesis of an Exceptionally Stable and Highly Porous Metal-Organic Framework. *Nature* **1999**, *402*, 276–279.

(6) Chae, H. K.; Siberio-Pérez, D. Y.; Kim, J.; Go, Y. B.; Eddaoudi, M.; Matzger, A. J.; O'Keeffe, M.; Yaghi, O. M. A Route to High Surface Area, Porosity and Inclusion of Large Molecules in Crystals. *Nature* **2004**, *427*, 523–527.

(7) Furukawa, H.; Ko, N.; Go, Y. B.; Aratani, N.; Choi, S. B.; Choi, E.; Yazaydin, O. A.; Snurr, R. Q.; O'Keeffe, M.; Kim, J.; Yaghi, O. M. Ultrahigh Porosity in Metal-Organic Frameworks. *Science* **2010**, *329*, 424–428.

(8) Klein, N.; Senkovska, I.; Gedrich, K.; Stoeck, U.; Henschel, A.; Mueller, U.; Kaskel, S. A Mesoporous Metal-Organic Framework. *Angew. Chem. Int. Ed.* **2009**, *48*, 9954–9957.

(9) Jiang, J.; Furukawa, H.; Zhang, Y.-B.; Yaghi, O. M. High Methane Storage Working Capacity in Metal-Organic Frameworks with Acrylate Links. *J. Am. Chem. Soc.* **2016**, *138*, 10244–10251.

(10) Liu, L.; Konstas, K.; Hill, M. R.; Telfer, S. G. Programmed Pore Architectures in Modular Quaternary Metal-Organic Frameworks. *J. Am. Chem. Soc.* **2013**, *135*, 17731–17734.

(11) Koh, K.; Wong-Foy, A. G.; Matzger, A. J. A Crystalline Mesoporous Coordination Copolymer with High Microporosity. *Angew. Chem. Int. Ed.* **2008**, *47*, 677–680.

(12) Koh, K.; Van Oosterhout, J. D.; Roy, S.; Wong-Foy, A. G.; Matzger, A. J. Exceptional surface area from coordination copolymers derived from two linear linkers of differing lengths. *Chem. Sci.* **2012**, *3*, 2429–2432.

(13) Gomez-Cualdron, D. A.; Gutov, O. V.; Krungleviciute, V.; Borah, B.; Mondloch, J. E.; Hupp, J. T.; Yildirim, T.; Farha, O. K.; Snurr, R. Q. Computational Design of Metal-Organic Frameworks Based on Stable Zirconium Building Units for Storage and Delivery of Methane. *Chem. Mater.* **2014**, *26*, 5632–5639.

(14) Alezi, D.; Spanopoulos, I.; Tsangarakis, C.; Shkurenko, A.; Adil, K.; Belmabkhout, Y.; O'Keeffe, M.; Eddaoudi, M.; Trikalitis, P. N. Reticular Chemistry at Its Best: Directed Assembly of Hexagonal Building Units into the Awaited Metal-Organic Framework with the Intricate Polybenzene Topology, pbz-MOF. *J. Am. Chem. Soc.* **2016**, *138*, 12767–12770.

(15) Pang, J.; Jiang, F.; Wu, M.; Yuan, D.; Zhou, K.; Qian, J.; Su, K.; Hong, M. Coexistence of cages and one-dimensional channels in a porous MOF with high H_2 and CH_4 uptakes. *Chem. Commun.* **2014**, *50*, 2834–2836.

(16) Chui, S. S.-Y.; Lo, S. M.-F.; Charmant, J. P. H.; Orpen, G. A.; Williams, I. D. A Chemically Functionalizable Nanoporous Material $[Cu_3(TMA)_2(H_2O)_3]_n$. *Science* **1999**, *283*, 1148–1150.

(17) Wang, Z.; Zheng, B.; Liu, H.; Yi, P.; Li, X.; Yu, X.; Yun, R. A highly porous 4,4-paddlewheel-connected NbO-type metal-organic framework with a large gas-uptake capacity. *Dalton Trans.* **2013**, *42*, 11304–11311.

(18) Yan, Y.; Kolokolov, D. I.; da Silva, I.; Stepanov, A. G.; Blake, A. J.; Dailly, A.; Manuel, P.; Tang, C. C.; Yang, S.; Schröder, M. Porous Metal-Organic Polyhedral Frameworks with Optimal Molecular Dynamics and Pore Geometry for Methane Storage. *J. Am. Chem. Soc.* **2017**, *139*, 13349–13360.

(19) Chen, B.; Ockwig, N. W.; Millward, A. R.; Contreras, D. S.; Yaghi, O. M. High H_2 Adsorption in a Microporous Metal-Organic Framework with Open Metal Sites. *Angew. Chem. Int. Ed.* **2005**, *44*, 4745–4749.

(20) Lin, X.; Jia, J.; Zhao, X.; Thomas, M.; Blake, A. J.; Walker, G. S.; Champness, N. R.; Hubberstey, P.; Schröder, M. High H_2 Adsorption by Coordination-Framework Materials. *Angew. Chem. Int. Ed.* **2006**, *45*, 7358–7364.

(21) Lu, Z.; Du, L.; Tang, K.; Bai, J. High H_2 and CH_4 Adsorption Capacity of a Highly Porous (2,3,4)-Connected Metal-Organic Framework. *Cryst. Growth Des.* **2013**, *13*, 2252–2255.

(22) Zhang, M.; Li, B.; Li, Y.; Wang, Q.; Zhang, W.; Chen, B.; Li, S.; Pan, Y.; You, X.; Bai, J. Finely tuning MOFs towards high performance in C_2H_2 storage: synthesis and properties of a new MOF-505 analogue with an inserted amide functional group. *Chem. Commun.* **2016**, *52*, 7241–7244.

(23) Zhang, M.; Chen, C.; Wiang, Q.; Fu, W.; Huang, K.; Zhou, W. A metal-organic framework functionalized with piperazine exhibiting enhanced CH_4 storage. *J. Mater. Chem. A* **2017**, *5*, 349–354.

(24) Zhang, M.; Zhou, W.; Pham, T.; Forrest, K. A.; Liu, W.; He, Y.; Wu, H.; Yildirim, T.; Chen, B.; Space, B.; Pan, Y.; Zaworotko, M. J.; Bai, J. Fine Tuning of MOF-505 Analogues to Reduce Low-Pressure Methane Uptake and Enhance Methane Working Capacity. *Angew. Chem. Int. Ed.* **2017**, *56*, 11426–11430.

(25) Lin, X.; Telepeni, I.; Blake, A. J.; Dailly, A.; Brown, C. M.; Simmons, J. M.; Zoppi, M.; Walker, G. S.; Thomas, K. M.; Mays, T. J.; Hubberstey, P.; Champness, N. R.; Schröder, M. High Capacity Hydrogen Adsorption in Cu(II) Tetracarboxylate Framework Materials: The Role of Pore Size, Ligand Functionalization, and Exposed Metal Sites. *J. Am. Chem. Soc.* **2009**, *131*, 2159–2171.

(26) Farha, O. K.; Wilmer, C. E.; Eryazici, I.; Hauser, B. G.; Parilla, P. A.; O'Neill, K.; Sarjeant, A. A.; Nguyen, S. T.; Snurr, R. Q.; Hupp, J. T. Designing Higher Surface Area Metal-Organic Frameworks: Are Triple Bonds Better Than Phenyls? *J. Am. Chem. Soc.* **2012**, *134*, 9860–9863.

(27) Wilmer, C. E.; Farha, O. K.; Yildirim, T.; Eryazici, I.; Krungleviciute, V.; Sarjeant, A. A.; Snurr, R. Q.; Hupp, J. T. Gram-scale, high-yield synthesis of a robust metal-organic framework for storing methane and other gases. *Energy Environ. Sci.* **2013**, *6*, 1158–1163.

(28) Kennedy, R. D.; Krungleviciute, V.; Clingerman, D. J.; Mondloch, J. E.; Peng, Y.; Wilmer, C. E.; Sarjeant, A. A.; Snurr, R. Q.; Hupp, J. T.; Yildirim, T.; Farha, O. K.; Mirkin, C. A. Carborane-Based Metal-Organic Framework with High Methane and Hydrogen Storage Capacities. *Chem. Mater.* **2013**, *25*, 3539–3543.

(29) Barin, G.; Krungleviciute, V.; Gomez-Cualdron, D. A.; Sarjeant, A. A.; Snurr, R. Q.; Hupp, J. T.; Yildirim, T.; Farha, O. K. Isoreticular Series of (3,24)-Connected Metal-Organic Frameworks: Facile Synthesis and High Methane Uptake Properties. *Chem. Mater.* **2014**, *26*, 1912–1917.

(30) Wang, X.-S.; Ma, S.; Rauch, K.; Simmons, J. M.; Yuan, D.; Wang, X.; Yildirim, T.; Cole, W. C.; López, J. J.; de Meijere, A.; Zhou, H.-C. Metal-Organic Frameworks Based on Double-Bond-Coupled Di-Isophthalate Linkers with High Hydrogen and Methane Uptakes. *Chem. Mater.* **2008**, *20*, 3145–3152.

(31) Ma, S.; Sun, D.; Simmons, J. M.; Collier, C. D.; Yuan, D.; Zhou, H.-C. Metal-Organic Framework from an Anthracene Derivative Containing Nanoscopic Cages Exhibiting High Methane Uptake. *J. Am. Chem. Soc.* **2008**, *130*, 1012–1016.

(32) Zhao, D.; Yuan, D.; Sun, D.; Zhou, H.-C. Stabilization of Metal-Organic Frameworks with High Surface Areas by the Incorporation of Mesocavities with Microwindows. *J. Am. Chem. Soc.* **2009**, *131*, 9186–9188.

(33) Yuan, D.; Zhao, D.; Sun, D.; Zhou, H.-C. An Isoreticular Series of Metal-Organic Frameworks with Dendritic Hexacarboxylate Ligands and Exceptionally High Gas-Uptake Capacity. *Angew. Chem. Int. Ed.* **2010**, *49*, 5357–5361.

(34) Yan, Y.; Telepeni, I.; Yang, S.; Lin, X.; Kockelmann, W.; Dailly, A.; Blake, A. J.; Lewis, W.; Walker, G. S.; Allan, D. A.; Barnett, S. A.; Champness, N. R.; Schröder, M. Metal-Organic Polyhedral Frameworks: High H_2 Adsorption Capacities and Neutron Powder Diffraction Studies. *J. Am. Chem. Soc.* **2010**, *132*, 4092–4094.

(35) Farha, O. K.; Yazaydin, O. A.; Eryazici, I.; Malliakas, C. D.; Hauser, B. G.; Kanatzidis, M. G.; Nguyen, S. T.; Snurr, R. Q.; Hupp, J. T. De novo synthesis of a metal-organic framework material featuring ultrahigh surface area and gas storage capacities. *Nat. Chem.* **2010**, *2*, 944–948.

(36) Guo, Z.; Wu, H.; Srinivas, G.; Zhou, Y.; Xiang, S.; Chen, Z.; Yang, Y.; Zhou, W.; O'Keeffe, M.; Chen, B. A Metal-Organic Framework with Optimized Open Metal Sites and Pore Spaces for High Methane Storage at Room Temperature. *Angew. Chem. Int. Ed.* **2011**, *50*, 3178–3181.

(37) Xu, G.; Li, B.; Wu, H.; Zhou, W.; Chen, B. Construction of ntt-Type Metal-Organic Framework from C_2-Symmetry Hexacarboxylate Linker for Enhanced Methane Storage. *Cryst. Growth Des.* **2017**, *17*, 4795–4800.

(38) Li, B.; Wen, H.-M.; Wang, H.; Wu, H.; Tyagi, M.; Yildirim, T.; Zhou, W.; Chen, B. A Porous Metal-Organic Framework with Dynamic Pyrimidine Groups Exhibiting Record High Methane Storage Working Capacity. *J. Am. Chem. Soc.* **2014**, *136*, 6207–6210.

(39) Wen, H.-M.; Li, B.; Yuan, D.; Wang, H.; Yildirim, T.; Zhou, W.; Chen, B. A porous metal-organic framework with an elongated anthracene derivative exhibiting a high working capacity for the storage of methane. *J. Mater. Chem. A* **2014**, *2*, 11516–11522.

(40) Chang, G.; Li, B.; Wang, H.; Bao, Z.; Yildirim, T.; Yao, Z.; Xiang, S.; Chen, B. A microporous metal-organic framework with polarized trifluoromethyl groups for high methane storage. *Chem. Commun.* **2015**, *51*, 14789–14792.

(41) Wen, H.-M.; Li, B.; Li, L.; Lin, R.-B.; Zhou, W.; Qian, G.; Chen, B. A Metal-Organic Framework with Optimized Porosity and Functional Sites for High Gravimetric and Volumetric Methane Storage Working Capacities. *Adv. Mater.* **2018**, *30*, 1704792.

(42) Rao, X.; Cai, J.; Yu, J.; He, Y.; Wu, C.; Zhou, W.; Yildirim, T.; Chen, B.; Qian, G. A microporous metal-organic framework with both open metal and Lewis basic pyridyl sites for high C_2H_2 and CH_4 storage at room temperature. *Chem. Commun.* **2013**, *49*, 6719–6721.

(43) Cai, J.; Rao, X.; He, Y.; Yu, J.; Wu, C.; Zhou, W.; Yildirim, T.; Chen, B.; Qian, G. A highly porous NbO type metal-organic framework constructed from an expanded tetracarboxylate. *Chem. Commun.* **2014**, *50*, 1552–1554.

(44) Kong, G.-Q.; Han, Z.-D.; He, Y.; Ou, S.; Zhou, W.; Yildirim, T.; Krishna, R.; Zou, C.; Chen, B.; Wu, C.-D. Expanded Organic Building Units for the Construction of Highly Porous Metal-Organic Frameworks. *Chem.–Eur. J.* **2013**, *19*, 14886–14894.

(45) Vanduyfhuys, L.; Vandenbrande, S.; Verstraelen, T.; Schmid, R.; Waroquier, M.; Van Speybroeck, V. QuickFF: A Program for a Quick and Easy Derivation of Force Fields for Metal-Organic Frameworks from Ab Initio Input. *J. Comput. Chem.* **2015**, *36*, 1015–1027.

(46) Vanduyfhuys, L.; Vandenbrande, S.; Wieme, J.; Waroquier, M.; Verstraelen, T.; Van Speybroeck, V. Extension of the QuickFF force field protocol for an improved accuracy of structural, vibrational, mechanical and thermal properties of metal-organic frameworks. *J. Comput. Chem.* **2018**, *39*, 999–1011.

(47) Frisch, M. J.; Trucks, G. W.; Schlegel, H. B.; Scuseria, G. E.; Robb, M. A.; Cheeseman, J. R.; Scalmani, G.; Barone, V.; Petersson, G. A.; Nakatsuji, H.; Li, X.; Caricato, M.; Marenich, A. V.; Bloino, J.; Janesko, B. G.; Gomperts, R.; Mennucci, B.; Hratchian, H. P.; Ortiz, J. V.; Izmaylov, A. F.; Sonnenberg, J. L.; Williams-Young, D.; Ding, F.; Lipparini, F.; Egidi, F.; Goings, J.; Peng, B.; Petrone, A.; Henderson, T.;

Ranasinghe, D.; Zakrzewski, V. G.; Gao, J.; Rega, N.; Zheng, G.; Liang, W.; Hada, M.; Ehara, M.; Toyota, K.; Fukuda, R.; Hasegawa, J.; Ishida, M.; Nakajima, T.; Honda, Y.; Kitao, O.; Nakai, H.; Vreven, T.; Throssell, K.; Montgomery, J. A., Jr.; Peralta, J. E.; Ogliaro, F.; Bearpark, M. J.; Heyd, J. J.; Brothers, E. N.; Kudin, K. N.; Staroverov, V. N.; Keith, T. A.; Kobayashi, R.; Normand, J.; Raghavachari, K.; Rendell, A. P.; Burant, J. C.; Iyengar, S. S.; Tomasi, J.; Cossi, M.; Millam, J. M.; Klene, M.; Adamo, C.; Cammi, R.; Ochterski, J. W.; Martin, R. L.; Morokuma, K.; Farkas, O.; Foresman, J. B.; Fox, D. J. Gaussian16 Revision E.01. 2016; Gaussian Inc. Wallingford CT.

(48) Becke, A. D. Density-Functional Thermochemistry. III. The Role of Exact Exchange. *J. Chem. Phys.* **1993**, *98*, 5648–5652.

(49) Krishnan, R.; Binkley, J. S.; Seeger, R.; Pople, J. A. Self-Consistent Molecular Orbital Methods. 20. Basis Set for Correlated Wave-Functions. *J. Chem. Phys.* **1980**, *72*, 650–654.

(50) Hay, P. J.; Wadt, W. R. Ab Initio Effective Core Potentials for Molecular Calculations. Potentials for the Transition Metal Atoms Sc to Hg. *J. Chem. Phys.* **1985**, *82*, 270.

(51) Verstraelen, T.; Vandenbrande, S.; Heidar-Zadeh, F.; Vanduyfhuys, L.; Van Speybroeck, V.; Waroquier, M.; Ayers, P. W. Minimal Basis Iterative Stockholder: Atoms-in-Molecules for Force-Field Development. *J. Chem. Theory Comput.* **2016**, *12*, 3894–3912.

(52) Perdew, J. P.; Burke, K.; Ernzerhof, M. Generalized Gradient Approximation Made Simple. *Phys. Rev. Lett.* **1996**, *77*, 3865–3868.

(53) Mortensen, J. J.; Hansen, L. B.; Jacobsen, K. W. Real-Space Grid Implementation of the Projector Augmented Wave Method. *Phys. Rev. B* **2005**, *71*, 035109.

(54) Allinger, N. L.; Yuh, Y. H.; Lii, J. H. Molecular Mechanics. The MM3 Force Field for Hydrocarbons. 1. *J. Am. Chem. Soc.* **1989**, *111*, 8551–8566.

(55) Vanduyfhuys, L.; Vandenbrande, S.; Wieme, J.; Waroquier, M.; Verstraelen, T.; Van Speybroeck, V. Extension of the QuickFF Force Field Protocol for an Improved

Accuracy of Structural, Vibrational, Mechanical and Thermal Properties of Metal-Organic Frameworks. *J. Comput. Chem.* **2018**, *39*, 999–1011.

(56) Lamaire, A.; Wieme, J.; Rogge, S. M. J.; Waroquier, M.; Van Speybroeck, V. On the Importance of Anharmonicities and Nuclear Quantum Effects in Modelling the Structural Properties and Thermal Expansion in MOF-5. *J. Chem. Phys.* **2019**, *150*, 094503.

(57) Chen, J.; Martínez, T. J. QTPIE: Charge Transfer with Polarization Current Equalization. A Fluctuating Charge Model with Correct Asymptotics. *Chem. Phys. Lett.* **2007**, *438*, 315–320.

(58) Lii, J. H.; Allinger, N. L. Molecular Mechanics. The MM3 Force Field for Hydrocarbons. 3. The van der Waals Potentials and Crystal Data for Aliphatic and Aromatic Hydrocarbons. *J. Am. Chem. Soc.* **1989**, *111*, 8576–8582.

(59) Allinger, N. L.; Zhou, X.; Bergsma, J. Molecular Mechanics Parameters. *J. Mol. Struc.-THEOCHEM* **1994**, *312*, 69–83.

(60) Sun, H. COMPASS: An ab Initio Force-Field Optimized for Condensed-Phase Applications - Overview with Details on Alkane and Benzene Compounds. *J. Phys. Chem. B* **1998**, *102*, 7338–7364.